Remote Sensing for Earth Observation and Surveillance
Assignment #2

Fontan Anna (945648)

Notation

Dimensional quantities:

$\Delta\psi$	Antenna azimuthal beamwidth	[deg]
Δx_{ANT}	Spatial sampling of synthetic aperture	[m]
θ_i	Incident angle	[deg]
λ	Wavelength	[m]
μ_E	Earth gravitational parameter	$[\frac{m^3}{s^2}]$
ρ_r	Range resolution	[m]
ρ_x	Ground: azimuth resolution	[m]
ρ_y	Ground: range resolution	[m]
ψ	Interferometric phase	[deg]
A_{ANT}	Antenna area	[m^2]
A_e	Antenna equivalent area	[m^2]
A_s	Synthetic aperture lenght	[m]
B	Bandwidth	[Hz]
c	Speed of light	$[\frac{m}{s}]$
b_n	Normal baseline	[m]
f_0	Carrier frequency	[Hz]
GRS	Ground range swath	[mm]
H	Altitude	[m]
L_{tot}	Total length of the orbit	[m]
L_x	Antenna azimuth-wise length	[m]
L_z	Antenna zenith-wise length	[m]
N_0	Noise power density	[J]
P_{rx}	Received power	[W]
P_{tx}	Transmitted power	[W]
R	Ground range	[m]
R_e	Earth radius	[m]
T_g	Transmitted pulse duration	[s]
v_{SAR}	SAR orbital velocity	$[\frac{m}{s}]$
y	Ground range	[m]
z	Terrain topography	[m]
z_{amb}	Height of ambiguity	[m]

Non-dimensional quantities

γ	Interferometric coherence	[-]
η	Antenna efficiency	[-]
σ^0	Backscatter coefficient	[dB/-]
σ^0_{NESZ}	NESZ	[dB/-]
d_c	Duty cycle	[-]
F	Receiver noise figure	[dB/-]
$f_{tx/rx}$	Antenna pattern	[-]
G	Antenna gain	[dB/-]
N_p	Number of targets	[-]
N_τ	Effective number of pulses	[-]

Symbols

1D-ACC	1D Azimuth Cross-Correlation
CRB	Cramér-Rao Bound
DFT	Discrete Fourier Transform
NESZ	Noise Equivalent Sigma Zero
PRF	Pulse Repetition Frequency
PRI	Pulse Repetition Interval
RCS	Radar Cross Section
SNR	Signal to Noise Ratio
TDBP	Time Domain Back Projection

1 Problem 1: a SAR from scratch

1.1 Determine all relevant system parameters, including: approximate antenna size, radiated peak power, transmitted bandwidth, transmitted pulse duration, PRF, length of the synthetic aperture

In this section a basic design for a SAR system operating in Low Earth Orbit (LEO) is carried out. The system is required to take into account the following parameters, reported in Tab. 1.

Table 1: Data

Parameter	Value	Parameter	Value
H	500 km	f_0	9.65 GHz
R_e	6378.1 km	F_{dB}	5 dB
η	0.7	d_c	0.2
θ_i	30 deg	σ_{NESZ}	- 22 dB
ρ_x	3 m	GRS	45 km
ρ_y	3 m		

The geometrical properties (the minimum and maximum slant ranges and $\Delta\theta$) have been evaluated through the reference system reported in Fig. 1; one can notice indeed that all of them strongly depend on the altitude and on the ground range swath; equivalently, the minimum and maximum ground ranges can be evaluated as well.

$$R_{\text{min}} = \frac{H}{\cos\theta_i} \tag{1}$$

$$R_{\text{max}} = \sqrt{H^2 + (\text{GRS} + R_{\text{min}}\sin\theta_i)^2} \tag{2}$$

$$\Delta\theta = \arccos\left(\frac{H}{r_{\text{max}}}\right) - \theta_i \tag{3}$$

$$\rho_r = \rho_y \sin\theta_i \tag{4}$$

$$y_{\text{min}} = H\tan\theta_i \tag{5}$$

$$y_{\text{max}} = y_{\text{min}} + \text{GRS} \tag{6}$$

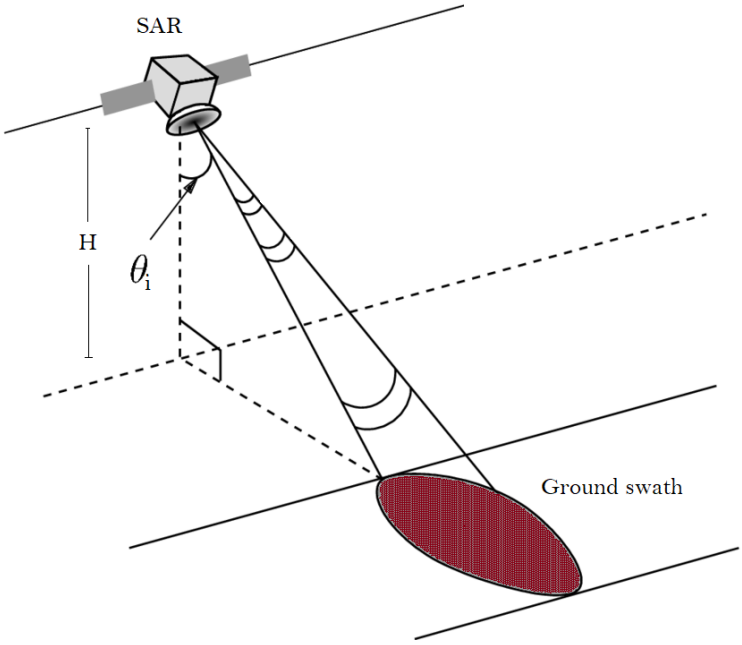

Figure 1: Geometric characteristics of SAR satellite [2]

Moreover, the other relevant parameters, i.e. L_x, L_z, A_s, A_{ANT}, A_e, Δx_{ANT}, λ, G, B and v_{SAR} have been evaluated as follows:

$$L_x = 2\rho_x = \frac{\lambda}{\Delta\psi} \tag{7}$$

$$L_z = \frac{\lambda}{\Delta\theta} \tag{8}$$

$$\Delta x_{ANT} = \frac{\rho_x}{2} \tag{9}$$

$$\lambda = \frac{c}{f_0} \tag{10}$$

$$A_{ANT} = L_x L_z \tag{11}$$

$$G = \eta \frac{4\pi}{\lambda^2} A_{ANT} = \frac{4\pi}{\lambda^2} A_e \tag{12}$$

$$B = \frac{c}{2\rho_r} \tag{13}$$

$$v_{SAR} = \sqrt{\frac{\mu_E}{R_E + H}} \tag{14}$$

Once these quantities are known the followings can be computed too:

$$PRI = \frac{\Delta x_{ANT}}{v_{SAR}} \tag{15}$$

$$PRF = \frac{1}{PRI} \tag{16}$$

$$T_g = PRI \cdot d_c \tag{17}$$

$$N_\tau = \frac{A_s}{PRI v_{SAR}} \tag{18}$$

Moreover, the selected data (Tab. 1) allows to avoid range and along track ambiguities; indeed, the inequalities below are valid:

$$\frac{2}{(r_{max} - r_{min})\, c} < PRI < \frac{\lambda}{2 v_{SAR} \Delta\psi} \tag{19}$$

$$\approx 159\mu s < PRI < 394\mu s \tag{20}$$

In order to evaluate the peak power too, the slant range has been set equal to R_{min} in order to have a reference value for the analysis. Therefore, the data of the Noise Equivalent Sigma Zero is exploited using Eq. 21, that can be obtained imposing SNR equal to 1 in the RADAR equation. Indeed, the NESZ can be written as a function of slant range R as:

$$\sigma^0_{NESZ} = \frac{\sin\theta_i}{\rho_x \rho_r} \frac{N_0}{N_\tau T_g P_{peak}} \frac{(4\pi R^2)^2}{G A_e f_{tx}^2} \tag{21}$$

where $f_{tx} = f_{tx}(\theta_i, \psi = 0) \approx 1$. The results are reported in Tab. 2.

Table 2: SAR relevant system parameters

Parameter	**Value**	**Parameter**	**Value**
B	99.93 MHz	P_{peak}	945.83 W
PRI	197.04 μs	L_x	6.00 m
PRF	5075.08 Hz	L_z	0.48 m
A_s	2989.38 m	T_g	39.41 μs

1.2 Discuss the choice of the focusing processor (is 1D-ACC enough?)

The problem analyses a SAR system; hence the focusing processor has to be chosen between a TDBP and a 1D-ACC (along-track compression) methods, since the DFT one for SAR cannot be implemented. Thus, a certain number of randomly fixed targets has been chosen, in order to simulate how the analysed system would behave using the satellite data reported in section 1.1.
In Tab. 3 the number of targets and the total length of the simulated orbit have been reported.

Table 3: Focusing processors data

Parameter	Value
N_p	15
L_{tot}	5981.36 m

From Fig. 2a and Fig. 2b one can notice that the both algorithms implementations in this simulated example lead to the identification of the targets; hence the two methods can be utilised. However, 1D-ACC method is "simpler" than TDBP. Indeed, to run this latter focusing processor, the GRS was reduced a lot, since TDBP is really demanding from a computation time point of view.
Fig. 3 shows how the two algorithms respond to the first target with respect to an ideal antenna (i.e. cardinal sine). Indeed, one can notice that TDBP (Fig. 3b) is the method that best approximates the ideal behaviour, but at the same time 1D-ACC (Fig. 3a) leads to quite similar results. Hence, in order to decide the focusing processor a trade-off has to be accounted for between the computational times and accuracy of the results; however, 1D-ACC not only lead to good approximations, but it is undoubtedly much faster than the other one. So the selected method in this case can be either 1D-ACC and TDBP, but in order to compute it using the full (or at least a long enough) range swath, the 1D-ACC has to be utilised to have a relatively fast enough response. Nonetheless, if the velocity of TDBP can be improved, that would be the method to exploit.

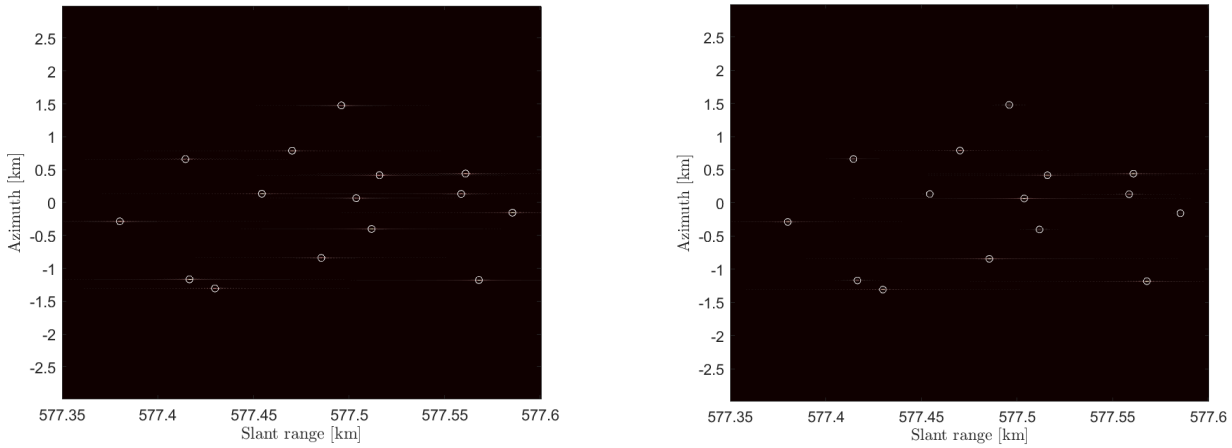

(a) 1D-ACC

(b) TDBP

Figure 2: Focusing processors

1.3 Discuss how to set the orbital separation between the two satellites to optimize estimation of terrain topography, and evaluate the expected estimation accuracy assuming a reference backscatter value σ^0 = - 15 dB

SAR Interferometry (InSAR) is a technology that permits to retrieve surface elevation by analysing the phase difference among different SAR images, which are acquired by flying a sensor along dissimilar orbits. In particular, the absolute value of the InSAR coherence provides a direct indication of the amount of phase noise at every pixel.
In this design, the variance $\sigma_{\Delta\phi}$ has been assumed equal to the Cramér-Rao Bound (CRB, Eq. 22), which expresses a lower bound of any possible unbiased estimator if the equivalent number of uncorrelated pixels (L_{eq}) within the averaging window is sufficiently high ($\approx L_{eq} > 10$); this assumption can be exploited since the design concerns an InSAR, so the CRB is an acceptable approximation of the phase noise variance.

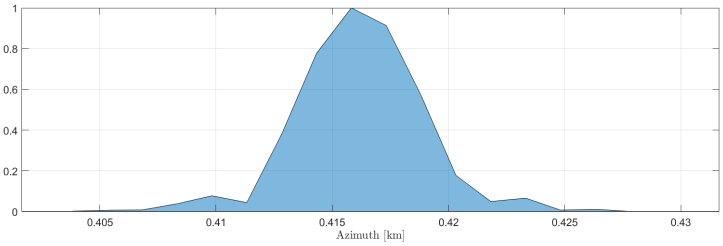

(a) 1D-ACC

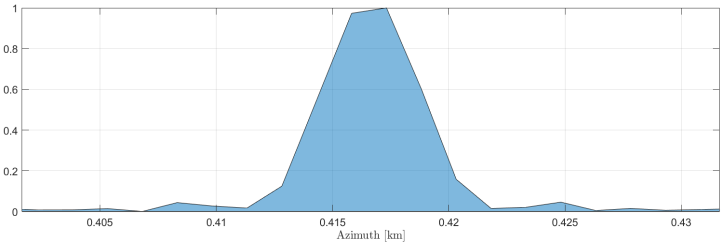

(b) TDBP

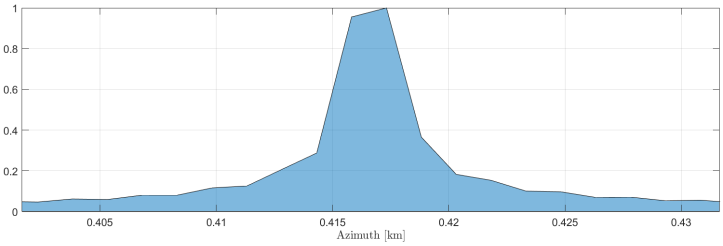

(c) Ideal

Figure 3: Analysis of pulse response after focusing

Therefore L_{eq} is set equal to 25, since the selected averaging window is [15 m x 15 m].

$$\sigma^2_{\Delta\phi} \geq \frac{1-|\gamma|^2}{2L_{eq}|\gamma|^2} \tag{22}$$

The interferometric coherence at every image pixel is defined as:

$$\gamma = \frac{E[I_2 I_1^*]}{\sqrt{E[|I_1|^2]E[|I_2|^2]}} \tag{23}$$

where $|\gamma| \leq 1$; in particular, if $|\gamma| = 1$ the two SAR images are perfectly correlated, whereas if $|\gamma| = 0$ they are completely uncorrelated. Indeed, a high value of the coherence is recommended, since as stated it is a measure of the degree of correlation between the SAR images.
Considering as decorrelation sources only the terrain and the noise (hence assuming bare surface and that the data are being acquired at the same time), the interferometric coherence can also be expressed as:

$$\gamma = \gamma_{\text{TERRAIN}} \cdot \gamma_{\text{SNR}} \tag{24}$$

where

$$\gamma_{\text{TERRAIN}} = 1 - \left|\frac{b_n}{b_{\text{CRITICAL}}}\right| \tag{25}$$

$$b_{\text{CRITICAL}} = \frac{B}{f_0} R \tan\theta_i \tag{26}$$

$$\gamma_{\text{SNR}} = \frac{\text{SNR}}{1+\text{SNR}} \tag{27}$$

From Eq. 25 the dependence of γ to the normal baseline between the two acquisitions (b_n) is underlined; b_{CRITICAL} corresponds instead to its critical value, i.e. the b_n for which the coherence is zero. In order to evaluate the received power and the SNR for Eq. 27, the RADAR equation has been used

once again, assuming that the transmitted power is the same as section 1.1.

$$P_{rx} = P_{tx} \frac{A_e G f_{tx}(\theta_i, 0)^2}{(4\pi R^2)^2} \text{RCS} \tag{28}$$

$$\text{SNR} = \frac{P_{rx} N_\tau T_g}{N_0} = \frac{\sigma^0}{\sigma^0_{\text{NESZ}}} = 5.012 \tag{29}$$

where $\text{RCS} = \sigma^0 \rho_x \rho_y$.

In order to optimise the estimation of terrain topography, σ_z has to be minimised choosing the proper normal baseline, where

$$\frac{b_n}{b_{\text{CRITICAL}}} \in [0, 1] \tag{30}$$

Moreover, the phase noise variance is linked to σ_z since, assuming still targets, the residual phase is directly linked to the target elevation:

$$\Delta\phi = \frac{4\pi}{\lambda} \frac{\Delta\theta}{\sin\theta_i} z = \frac{2\pi}{z_{amb}} z \tag{31}$$

hence:

$$\sigma_{\Delta\phi} = \frac{2\pi}{z_{amb}} \sigma_z \tag{32}$$

Table 4: Results for optimised σ_z

Parameter	**Value**	**Parameter**	**Value**
z_{amb}	2.99 m	$\Delta\Theta$	0.15 deg
$\sigma_{\Delta\phi}$	15.15 deg	γ	0.472
γ_{TERRAIN}	0.566	b_n	1499.28 m

From Fig. 6a one can notice that the minimum of σ_z can be identified within the ratio window (0.4, 0.5); moreover, from Tab. 7 one can notice that the optimised σ_z does not lead to the highest γ possible. Fig. 4 shows that if a high γ is desired as well, then the ratio should be at least lower than 0.2. However, since the design is focused on the error over the topography:

$$\sigma_{z,\text{OPT}} = \min(\sigma_z) = 0.126m \tag{33}$$

The highest values of σ_z (corresponding to $b_n/b_{\text{CRITICAL}} \to 0$ and $b_n/b_{\text{CRITICAL}} \to 1$) have been discharged from the analysis; indeed, as shown in Figs. 5a and 5b, the $\sigma_{\Delta\phi}$ should not be too high, as well as z_{amb}.

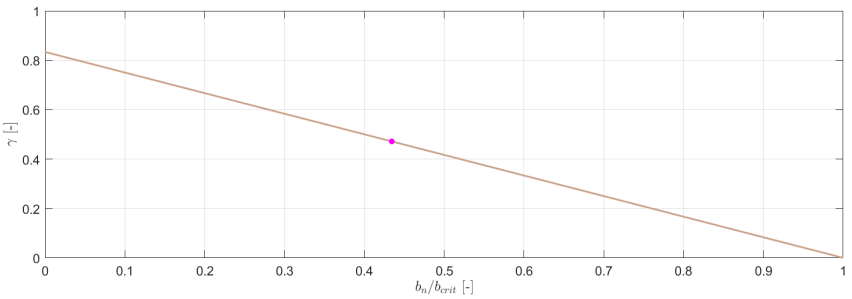

Figure 4: Interferometric coherence

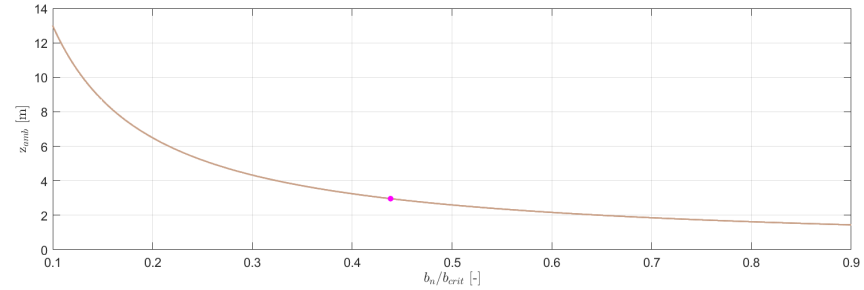

(a) z_{amb}

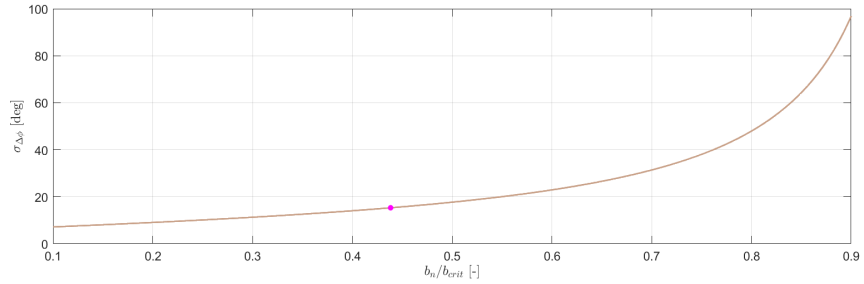

(b) $\sigma_{\Delta\phi}$

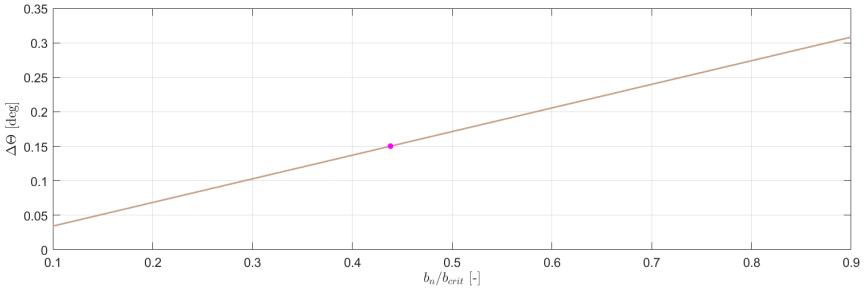

(c) $\Delta\Theta$

Figure 5: Ambiguous height, variance of the phase noise and difference of the nominal θ between the two orbits vs the ratio $b_n/b_{CRITICAL}$

2 Problem 2: some SAR processing

Fig. 7 shows the target figure, while the filter magnitude and phase in both time and frequency domains are represented from Fig. 8a to 8d. In particular, from Fig. 8a, one can notice that the signal g(t) has a quadratic phase and a constant amplitude in time too; indeed it is a chirp pulse, which phase is given by the sum of a linear and a quadratic in time terms.

2.1 Focus the raw data to produce a focused SAR image

To obtain a focused image, the following steps have been carried out:

1. the received data (D_{RAW}) have been filtered to generate a range-compressed data matrix (D_{RC}). In order to do so, a loop over the antenna positions has been exploited to compute the convolution of D_{RAW} with signal g(t). Fig. 9b shows the obtained matrix D_{RC};

2. different focusing algorithms have been utilised and then compared (the comparison is carried out in section 2.2); fig 11 shows the resulting image that has been obtained using a 1D matched filter.

To obtain the final image, Eqs. 4, 7, 9, 10 have been utilised, and the results are displayed in Tab. 5.

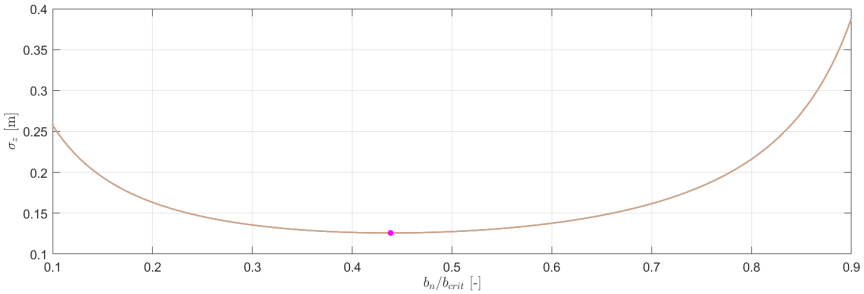

(a) σ_z zoomed

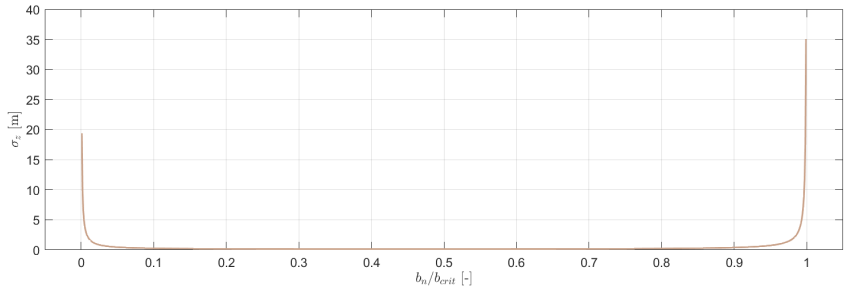

(b) σ_z

Figure 6: σ_z vs the ratio $b_n/b_{CRITICAL}$

Table 5: Results obtained

Parameter	**Value**	**Parameter**	**Value**
N_r	535	r_{max}	700.65 km
N_x	3003	r_{min}	699.85 km
L_x	10 m	λ	0.06 m

Where N_r and N_x are respectively the number of target range and antenna positions, linked to the fast and slow times.

2.2 Comment on the choice of the focusing algorithm and its performance in terms of image quality and computational burden

Different algorithms have been compared and they focus respectively by:

1. Discrete Fourier Transform (DFT): as expected, in this case this one does not lead to significant results (see Fig. 10) since the problem considers a SAR;
2. Time Domain Back Projection (TDBP): even tough it leads to a good image quality (see Fig. 12), at the same time it requires a high computational time;
3. 1D Azimuth Cross-Correlation (along-track compression): it leads to a focused image close to identical with TDBP one (see Fig. 11). Moreover, this is the simplest algorithm and it requires the fastest time to be computed, as shown in Tab. 6.

Indeed, as already specified in section 2.1, the chosen algorithm is the third one.

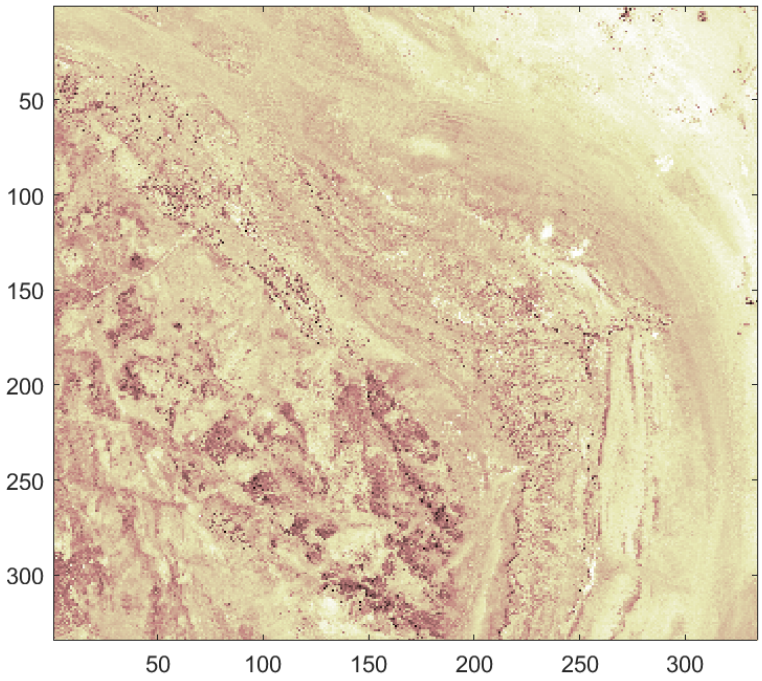

Figure 7: Target: Saudi Arabia

Table 6: Computation times of the analysed method

Method	CPU time [s]
1D-ACC	1.6445
TDBP	522.0436

2.3 Evaluate spatial resolution based on the acquisition parameters described in SAR data and check if it is consistent with the resulting focused image

Table 7: Range and azimuth resolutions

Parameter	Value
ρ_r	3 m
ρ_x	5 m

In Fig. 13a and Fig. 13b two different zoom-in are reported. One can observe indeed that the method is consistent with the theoretical results, which are enlightened in blue in the figures (see Tab. 7).

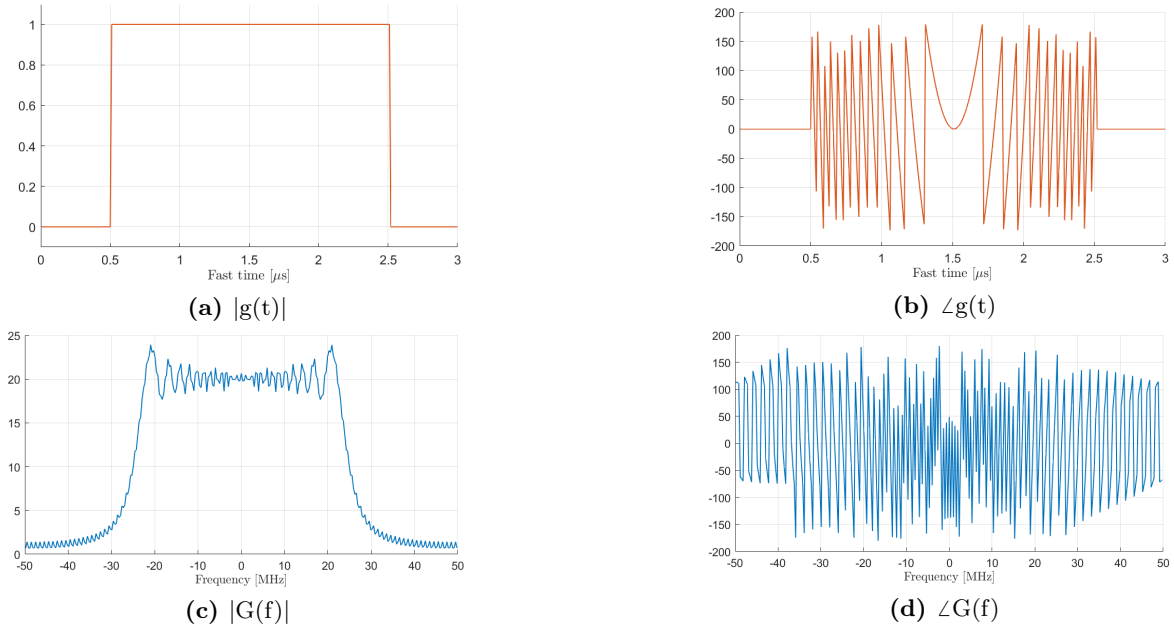

(a) |g(t)| **(b)** ∠g(t)

(c) |G(f)| **(d)** ∠G(f)

Figure 8: Transmitted pulse in time (Figs. 8a and 8b) and in frequency domains (Figs. 8c and 8d)

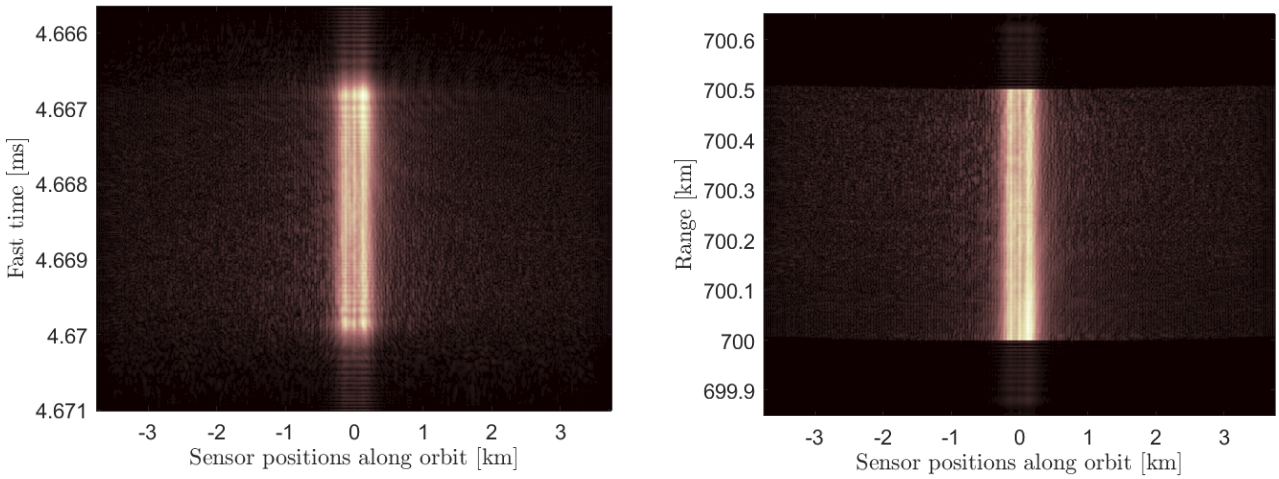

(a) raw: D_{RAW} **(b)** compressed range: D_{RC}

Figure 9: Data: raw (Fig. 9a) and after range compression (Fig. 9b)

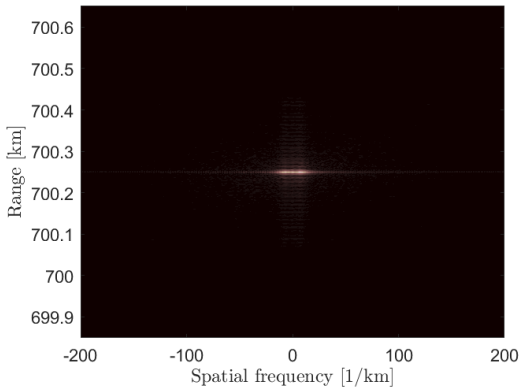

Figure 10: DFT

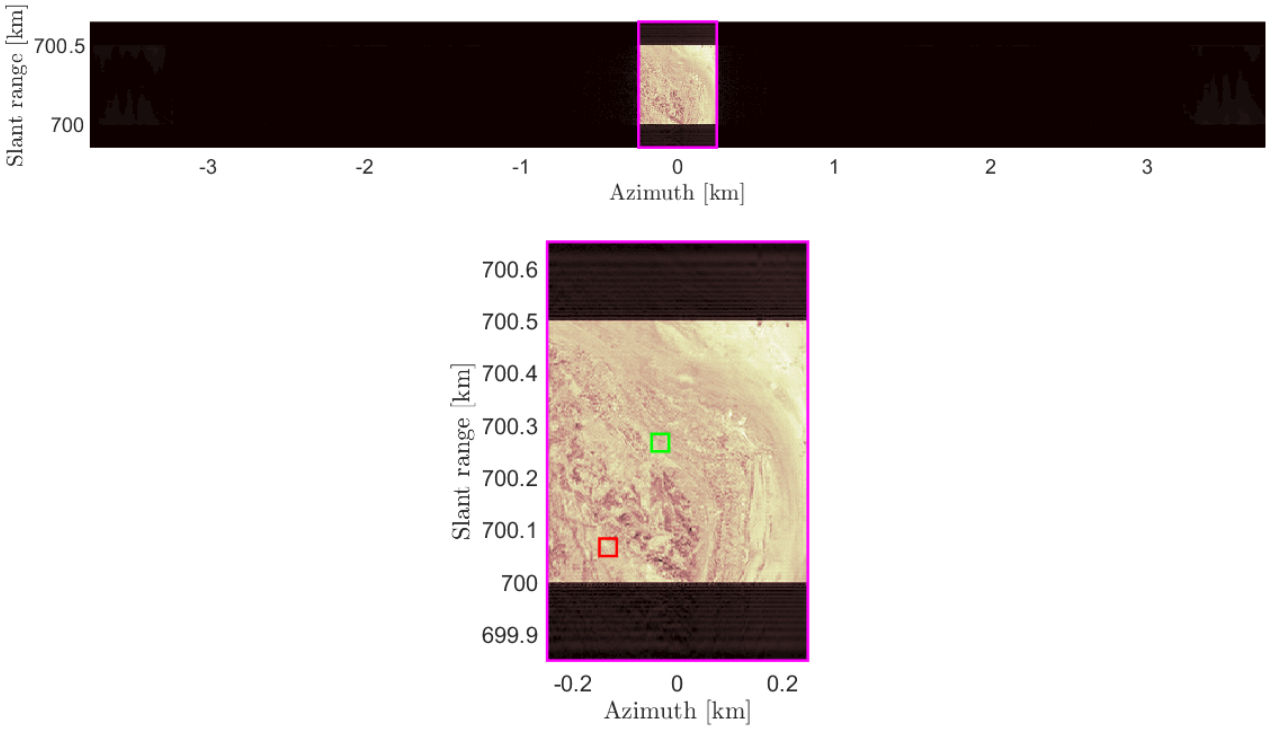

Figure 11: 1D-ACC

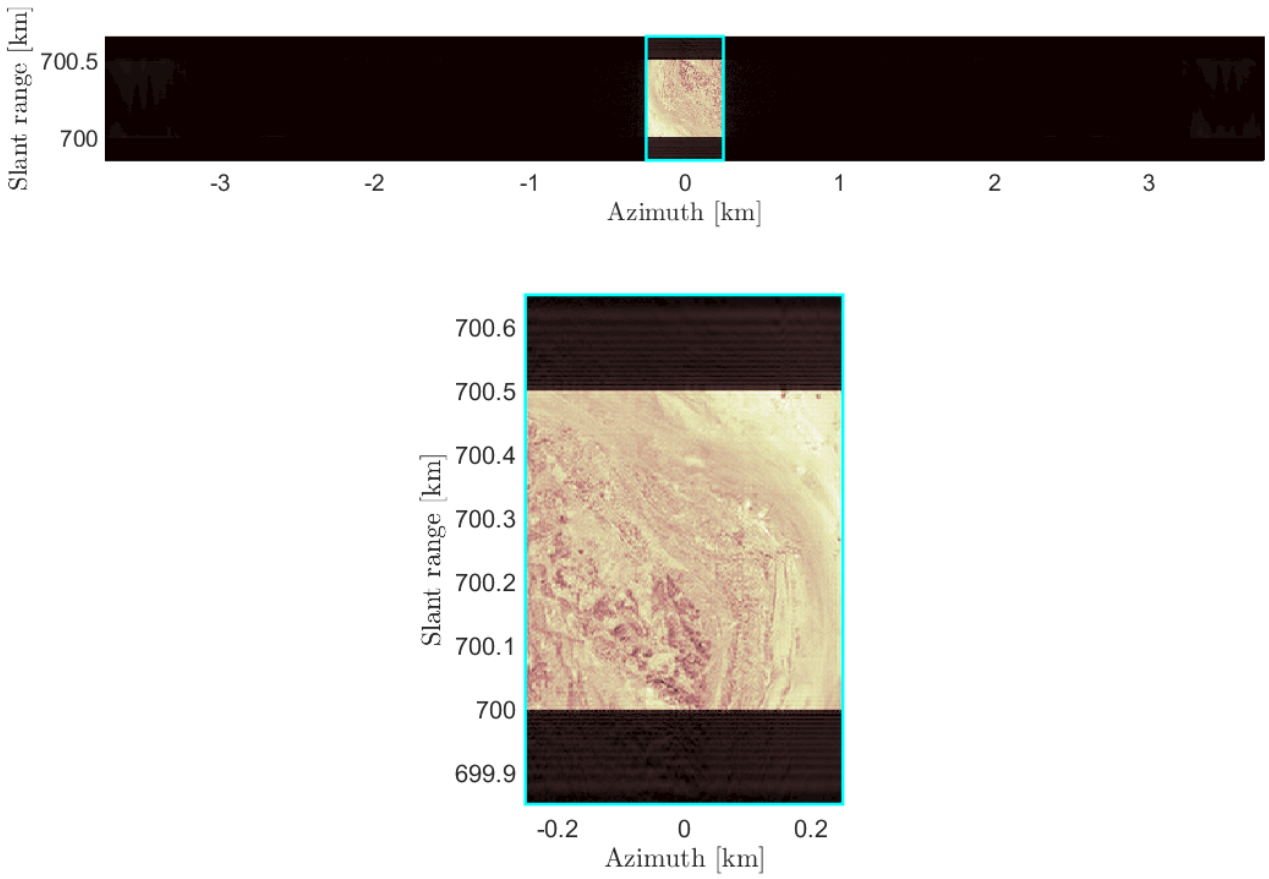

Figure 12: TDBP

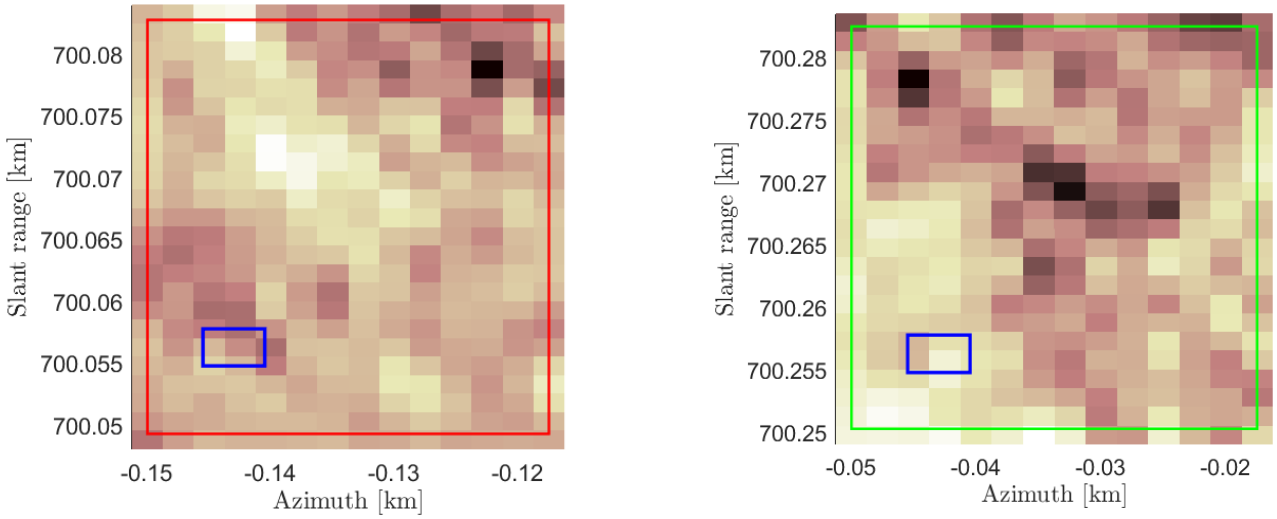

(a) First zoom-in

(b) Second zoom-in

Figure 13: Zooms of Fig. 11

References

[1] Andrea Monti Guarnieri *Electromagnetic Imaging*. 1^{st} ddition, October 2015, Politecnico di Milano, Dipartimento di Elettronica, Informazione e Bioingegneria

[2] Lauknes, Tom Rune (JOUR), *Rockslide Mapping in Norway by Means of Interferometric SAR Time Series Analysis*.

[3] A. Ferretti, A. Monti-Guarnieri, C. Prati, F. Rocca, Dipartimento di Elettronica ed Informazione, Politecnico di Milano, Italy, February 2007 (ESA). *InSAR Principles: Guidelines for SAR Interferometry Processing and Interpretation*.